INITIATION AND DISTRIBUTION OF MULTIPLE-SITE DAMAGE (MSD) IN A FUSELAGE LAP JOINT CURVED PANEL

Abubaker A. Ahmed
FAA-Drexel Fellowship Student
Department of Mechanical Engineering and Mechanics, Drexel University

John G. Bakuckas, Jr. and Paul W. Tan, AAR-400
FAA William J. Hughes Technical Center, Atlantic City International Airport, NJ

Jonathan Awerbuch, Alan C. Lau, and Tein-Min Tan
Faculty, Department of Mechanical Engineering and Mechanics, Drexel University

Abstract

A study has been conducted on the formation and evolution of multiple-site damage (MSD) emanating from the rivet holes in the lap joint of an initially undamaged full-scale fuselage curved panel subjected to fatigue loading. The experimental work was conducted at the Full-Scale Aircraft Structural Test Evaluation and Research (FASTER) facility located at the Federal Aviation Administration William J. Hughes Technical Center, Atlantic City International Airport, New Jersey. The FASTER test fixture is capable of applying an internal pressure and a combination of longitudinal, hoop, and frame loads to a curved panel to simulate realistic loading conditions an aircraft airframe experiences during an actual flight. The test panel was fully instrumented with strain gages. Quasi-static tests were conducted to ensure a proper load introduction into the panel. Nonlinear finite element analyses (FEA) were conducted to predict the strain distribution in the panel. FEA predictions were compared with the experimental data. The Self-Nulling Rotating Eddy-Current Probe system and the Remote Control Crack Monitoring system were used to detect and monitor crack formation and growth during the fatigue test. MSD cracks have been detected in the lap joint outer rivet row. The characteristics of these cracks are illustrated and discussed in detail.

Introduction

The widespread fatigue damage (WFD) phenomenon in aging aircraft is defined as the simultaneous presence of fatigue cracks at multiple structural details that are of sufficient size and density whereby the structure will no longer meet residual strength requirements. Multiple-site damage (MSD) is a type of WFD that is characterized by the simultaneous presence of fatigue cracks in the same structural element [1]. Riveted airframe joints are susceptible to MSD cracks, especially in aging transport aircraft. MSD cracks can initiate and grow along the rows of rivet holes in the joints and can linkup leading to potentially catastrophic loss of structural integrity.

In the 1988 Aloha Airlines accident, a 17-foot section of the fuselage crown of a Boeing 737-200 tore off during flight. Accident investigations revealed that the failure happened, in part, due to the linkup of MSD cracks emanating from rivet holes in a disbonded fuselage longitudinal lap joint [2]. The Aloha Airlines accident triggered research efforts on developing analytical and experimental models to study the initiation and growth of MSD cracks under fatigue loading and their effect on the fatigue life and residual strength of the fuselage structures. As part of these research efforts, the Full-Scale Aircraft Structural Test Evaluation and Research (FASTER) facility was established at the Federal Aviation Administration William J. Hughes Technical Center, Atlantic City International Airport, New Jersey. Previous curved panel studies conducted at the FASTER facility focused on the effect of MSD cracks on the fatigue crack growth and residual strength of the panels. Curved panels containing either longitudinal lap or circumferential butt joints with initial damages were tested [3 and 4].

The current study characterizes the initiation, distribution, and linkup of MSD cracks. A pristine curved fuselage panel containing a longitudinal lap joint was tested. The panel, which did not contain any initial damage, was subjected to constant-amplitude fatigue loading simulating the fuselage cabin pressurization condition. Quasi-static tests were conducted prior to the fatigue test to ensure a proper load introduction from the fixture to the panel. Nondestructive inspection (NDI) methods were used to closely monitor MSD initiation and growth during the fatigue test. Crack growth rates were calculated and compared with results from other similar studies. As of this writing, several sets of MSD have initiated on the panel. Residual strength test and posttest fractographic studies will be conducted after linkups of the MSD occur.

Test Facility

The curved panel test was conducted using the FASTER facility. The facility was established in 1999 to conduct fatigue and residual strength testing of full-scale fuselage curved panels. The facility hosts a test fixture that is capable of applying, to a full-scale curved panel, a combination of internal pressurization, hoop, longitudinal, frame, and shear loads to simulate real flight loading conditions encountered by an aircraft fuselage. A detailed description of the FASTER facility can be found in reference 4.

Two crack inspection methods, the Self-Nulling Rotating Eddy-Current Probe system and the Remote Control Crack Monitoring system (RCCM), have been used to detect and monitor crack formation and propagation. The rotating probe system is capable of detecting cracks that are hidden underneath countersunk rivet heads without removing the fastener. It has a 90% probability of detection for a 0.032″ crack [5]. The RCCM is a video data acquisition system consisting of two computer-controlled, high-precision x-y-z translation stages, each instrumented with a wide-field-of-view camera and a narrow-field-of-view camera. The combination of the two cameras allows monitoring of the entire panel surface at several levels of magnification, providing a field of view ranging from 0.05″ up to 14″. Each translation stage has a motion resolution of 0.00039″ (1 μm), allowing an accurate tracking of crack growth [2 and 4].

Experimental Procedure

Panel Configuration

A curved panel with dimensions of 120″ by 68″ and a radius of 68″ was used for this study. Figure 1 shows the schematic of the panel, which has a substructure of six frames, labeled as F1 through F6, in the circumferential direction, and seven stringers, labeled S1 through S7, in the longitudinal direction. The panel skin was made of 2024-T3 aluminum with a thickness of 0.063″. In the middle of the panel along stringer S4, there is a longitudinal lap joint with two 0.063″ thick 2024-T3 skin layers and two 0.025″ thick 2024-T3 finger doubler layers, connected together by four rivet rows, labeled A, B, C, and D, respectively, as shown in Figure 2. The rivet type for each row is also illustrated in the figure.

An elastomeric seal was bonded along the perimeter of the inner surface of the curved panel to attach to the pressure box of the FASTER fixture. The four edges of the panel are reinforced with aluminum doublers; holes are placed along the doublers so that the hoop and longitudinal load assemblies can be attached to the panel. The two ends of each frame, where the frame load assemblies are attached, are also reinforced with aluminum doublers.

The curved panel was fully instrumented with strain gages to monitor and record strain distribution during the test. Gage locations are shown in Figure 1. Several sets of back-to-back strain gages were installed in various locations on the panel to measure out-of-plane bending deformation. A cluster of 22 gages, including some back-to-back sets, were installed at the lap joint area near the center of the panel to closely monitor the strain distribution in that region.

Quasi-Static Tests

A series of quasi-static tests with various combinations of hoop, frame, longitudinal loads, and internal pressurization, as shown in Table 1, were conducted prior to the fatigue test. Loadings were applied to the panel using either water or air as the pressure media. Strains were measured and recorded at all strain gages and were compared with the results of a full-scale verification test, as well as predictions from the finite element analyses. The purpose of the quasi-static tests was to ensure proper load transfer from the fixture to the panel.

Fatigue Test

After the quasi-static tests were completed, a fatigue test was conducted with maximum loads shown in Table 1. The combination of internal pressure, hoop, frame, and longitudinal loads simulates a cabin pressurization condition. To accelerate the test, however, the maximum applied loads were higher than the typical operational loads of a fuselage structure. A load spectrum with underload cycles, as shown in Figure 3, was used to mark the fracture surfaces so that a fractographic study can be conducted after the completion of the test to reconstruct and map the crack growth histories. As of this writing, the panel has been subjected to more than 169,000 total fatigue cycles including 104,000 full-load (16 psi internal pressure) cycles. MSD cracks have been detected along rivet row A of the lap joint and at some of the rivets holding the shear clip to the skin at the shear clip cutouts at the frame-stringer intersections. The fatigue test will continue until the first linkup of MSD cracks occurs. The panel will then be subjected to a quasi-static load up to failure to determine the residual strength.

Crack Inspection

During the fatigue test, the curved panel has been continuously monitored for crack initiation and growth using the rotating probe system and the RCCM system. The rotating probe system was used to periodically inspect a total of 345 rivets in the panel for hidden cracks under the rivet heads. Of the 345 rivets, 285 are in rows A, B, and C of the lap joint. Rivet row D was not inspected with the rotating probe system due to limited accessibility. The remaining 60 are shear clip rivets, i.e., those holding the shear clips to the skin at the shear clip cutouts at the frame-stringer intersections. These 60 shear clip rivets are carrying high loads and are likely spots for MSD cracking initiation. A baseline inspection of the 345 rivets was conducted before the test began. Subsequent inspections were conducted on all 345 rivets at every 8,000 to 10,000 pressurization cycles, with a selected group of rivets being inspected more frequently at every 3,000 to 4,000 pressurization cycles. This group of rivets includes those located in the critical rivet row A of the lap joint, rivets that showed high amplitude in either the baseline or subsequent eddy-current inspections, and rivets that were leaking water. Once MSD cracks were visually detected, the inspections were conducted more frequently.

The RCCM system was used to perform high-magnification visual inspection of rivets that showed high eddy-current signals and those that were leaking water. After visual crack detection, the RCCM was used to measure the crack length. Still images and video tape recordings of the cracks at different stages were also taken.

Visual inspections of the skin edge and frame end doublers, skin and frame loading assemblies, and the inner surface of the panel were conducted periodically using a 10x magnifying glass. During the fatigue test, several failures occurred at locations on the doublers and loading assemblies. These failures were repaired as needed.

Analysis

A finite element model of the curved panel was developed, see Figure 4. Two-dimensional, four-noded, general-purpose shell elements with reduced integration and six degrees of freedom per node were used to model the skin, doublers, frames, and stringers; while three-dimensional, two-noded, linear beam elements with six degrees of freedom per node were used to model the rivets. The shear stiffness of the beam element was determined using the semiempirical equation [6]:

$$k_{shear} = \frac{E'd}{5 + 0.8\left(\frac{d}{t_1} + \frac{d}{t_2}\right)} \tag{1}$$

where $E' = 10.5 \times 10^6$ psi is the effective modulus of rivet material, $d = 0.1875''$ is the fastener diameter, and $t_1 = 0.063''$ and $t_2 = 0.063''$ are the thickness of the skin and substructure (shear clip or stringer), respectively.

Geometrical nonlinear analyses were conducted using the model shown in Figure 4 to predict the strain distributions in the panel under various quasi-static loading conditions given in Table 1. Boundary conditions and loads were applied to the finite element model to simulate the actual testing conditions. Pressure was applied to the inner surfaces of the model. Hoop and longitudinal loads were applied as concentrated forces. Concentrated forces were also applied at the frame ends to simulate the frame loads, as shown in Figure 4. Representative results and comparisons with the experimental data are presented in the following section. Additional analyses will be conducted using this model to predict crack initiation and growth.

Results and Discussions

Quasi-Static Tests

For each quasi-static loading condition listed in Table 1, four tests were conducted on the curved panel. Two test runs used water and the other two runs used air as the pressure medium. The strain distributions measured from all four tests were nearly identical [7], indicating that the FASTER fixture is reliable and the test data are highly repeatable using either water or air to pressurize the panel. The strain results were also compared with those obtained from full-scale verification tests conducted on an aft fuselage section of a narrow-body aircraft [7]. The good agreement between the two sets of results verified that loads were introduced properly into the panel through the loading mechanisms.

A geometrically nonlinear finite element analysis was conducted for each quasi-static test condition, and the strain predictions were compared with the experimental measurements at various gage locations. Typical results for gages located on a frame, on a stringer, and at a skin midbay area are presented in Figure 5, showing the strains as functions of applied load. There is excellent agreement between analysis and experiment. Similar agreement was obtained for results at other gage locations, indicating that the finite element model accurately predicts the responses of the primary structure of the curved panel under such loading conditions.

The curved panel, being subjected to a combination of loads that simulates a cabin pressurization condition, including internal pressure, hoop, longitudinal, and frame loads, should behave similar to a thin-walled pressure vessel with primarily in-plane deformation and very little bending. However, in the lap joint area, severe out-of-plane bending should be expected as a result of eccentricity due to the lap joint geometry. Several sets of back-to-back strain gages were installed at various locations in the panel to verify the local bending effect. Figure 6 shows the membrane and bending strain components, measured at two back-to-back gage sets, 33/34 at the midbay area and 39/39B at rivet row A, both in bay 3 of the curved panel. The membrane and bending components of strain are defined as:

$$\varepsilon_m = \frac{\varepsilon_o + \varepsilon_i}{2} \qquad \varepsilon_b = \frac{\varepsilon_o - \varepsilon_i}{2} \tag{2}$$

where

ε_m = membrane strain component

ε_b = bending strain component

ε_o = hoop strain on the skin outer surface

ε_i = hoop strain on the skin inner surface

It can be seen that the membrane strain components at both gage set locations differ slightly from each other. The bending strain component of gage set 33/34 is negligible, implying that the deformation in the midbay area is primarily in-plane. On the other hand, the results of gage set 39/39B indicate that a significant amount of local bending occurs near the lap joint area along rivet row A. Since ε_b has a negative value, the local bending in the lap joint area would produce very high tensile stress on the skin inner surface. This may explain why cracks normally initiate at the inner surface of the skin and propagate outward. Also shown in the figure are the finite element predictions, which are generally in good agreement with the experimental results.

Figure 7 compares the membrane and bending strain components measured at two other back-to-back gage sets, 68/68B and 70/70B, both in bay 2 of the curved panel, and those from a study on a flat panel with a similar lap joint configuration [8]. The gages in the flat panel study had been installed at the same location, relative to the lap joint, as gage set 70/70B shown in the figure. The comparisons clearly indicate that a higher bending strain is seen along rivet row A, and that the local bending effect at the lap joint in the curved panel is more than that in the flat panel. It is the local bending that causes MSD cracks to initiate at the rivet holes along rivet row A.

Fatigue Test

(a) Damage Evolution

During the initial inspection of the panel, several rivets in rivet row B in the lap joint area showed eddy-current signals higher than the threshold value of 15 mV. In the subsequent inspections, however, the signals from these rivets remained almost unchanged. These rivets, whose high eddy-current signals were probably due to manufacturing defects, are not included in the following discussion.

As of this writing, the panel has been subjected to 104,000 full-load (16 psi) fatigue cycles. Most of the high eddy-current signal rivets were in rivet row A. High signals were also obtained from the critical shear clip rivets nearest rivet row A. Visible damage was detected at some of the high eddy-current signal rivets. Figure 8 schematically shows the change in the eddy-current signal and the visible damage evolution in rivet row A and the critical shear clip rivets every 15,000 full-load cycles. In the figure, F1 through F6 denote the locations of the six frames, and F1-5 through F6-5 denote the six critical shear clip rivets. The five bays include 64 rivets in row A. Each block in Figure 8 shows the five bays separated by the six frames. It can be seen that, after the first 15,000 full-load cycles, only rivet A12 in bay 1 was showing high signals. Rivet A46 in bay 4 showed high signals after 30,000 cycles. A total of nine rivets, 13% of the rivets in row A, showed high signals after 45,000 full-load cycles.

Between 45,000 and 60,000 full-load cycles, two of the critical shear clip rivets, F4-5 and F5-5, started showing high eddy-current signals. A crack in the rivet head of A23 in bay 2 was detected after 51,600 full-load cycles. After about 75,000 full-load cycles, cracks were observed emanating from the rivet holes of the shear clip rivets F4-5 and F5-5. The locations where cracks were visually detected correlated very well with the eddy-current signals. In the meantime, rivet F3-5 was also beginning to show high signals. After 40,000 full-load cycles, 24% of the rivets in row A exhibited high eddy-current signals above the threshold.

Between 75,000 and 90,000 full-load cycles, rivet head cracks similar to that on rivet A23 were observed at five other rivets along rivet row A (all previously recorded high eddy-current signals). Skin cracks have also appeared on both sides of rivet A23, but at a distance from the edge of the rivet hole. These skin cracks propagated in both directions and eventually linked up with the rivet hole. More detailed discussion on these skin cracks will be given later. In addition, two cracks were observed at the rivet hole of the shear clip rivet F3-5, as well as several new cracks at rivets F4-5 and F5-5. After 90,000 full-load cycles, 27% of the rivets in row A exhibited high eddy-current signals above the threshold.

Between 90,000 and 104,000 full-load cycles, high eddy-current signals were detected at more rivets, but the only cracks that were showing appreciable growth were those linked up to rivet hole A23 and the two newly initiated cracks that linked up with rivet hole A22. The cracks at shear clip rivet holes F4-5 and F5-5, although detected first, were growing at a slower rate compared with cracks at rivet row A. It is anticipated that the two cracks propagating towards each other from rivets A22 and A23 will linkup. The fatigue test will be stopped after first crack linkup and the panel will be loaded quasi-statically up to failure to determine its residual strength. After 104,000 full-load cycles, 33% of the rivets in row A exhibited high eddy-current signals above the threshold.

The damage evolution process of rivet A23 is further illustrated in Figure 9 with a series of photographic images taken using the RCCM system. The full-load cycle number at which each image was taken is also shown in the figure. Damage in rivet A23 was first observed in the form of a rivet head crack. Subsequently, the crack grew along a curved path that seemed to follow the perimeter of the rivet stem, Figure 9(a). Water leakage from this crack indicates that it was a through-the-thickness crack. It is noted that the loading used in this study is much higher than what a fuselage would experience during normal service conditions. The rivets are not designed to sustain such high fatigue loads. Thus, it is believed that the rivet head crack initiated at the rivet shank-countersink interface due to the stress concentration in that area and propagated upwards to the surface. As the fatigue test continued, a through-the-thickness crack appeared on the right side of the rivet at a distance from the edge of the rivet hole, Figure 9(b). The through crack grew in both directions and eventually linked up with the rivet hole, Figure 9(c). At a later stage, another through-the-thickness crack appeared on the left side of the rivet, Figure 9(d). This crack also grew in both directions and linked up with the rivet hole, Figure 9(e). Finally, the rivet head crack also propagated to the edge of the rivet hole and joined the other two cracks to form a major crack that cuts through the rivet itself, Figure 9(f). A similar damage evolution process was observed at the neighboring rivet, A22.

(b) Eddy-Current Inspections

Figure 10 shows the eddy-current inspection results for rivet A23 up to 72,000 full-load cycles, which corresponds to the crack state shown in Figure 9(a). The highest signals were detected at around the -120° location, followed by another high value at around the +120° location. Recall that the first visually detected damage on the skin near rivet A23 was a through-the-thickness crack that occurred on the right side of the rivet, which eventually linked up with the rivet hole of A23 at -120° location. A similar crack was later observed on the left side of the rivet and linked up with the rivet hole at the +120° location. This indicates that the rotating probe system indeed detected hidden cracks initiated under the rivet head. It is plausible to assume that the high residual stress field near the rivet head resulting from the riveting process may have prevented these hidden cracks from propagating through the immediate vicinity of the rivet. This will be investigated through a posttest fractographic study of the crack surfaces and detailed finite element stress analyses.

Similar eddy-current inspection results and damage evolution process were observed at rivet A22 where the maximum signals were detected at around the +105° and -120° locations. Figure 11 shows the four maximum amplitudes of eddy-current signals, two each from rivets A22 and A23, as functions of the number of full-load fatigue cycles. The maximum amplitudes at which cracks on the left and right sides of rivets A22 and A23, denoted by A22L, A22R, A23L, and A23R, were first visually detected are also indicated in the figure by horizontal lines. The values of these maximum amplitudes range from 100 to

120 mV. It is noted that the cracks at shear clip rivets F4-5 and F5-5 were first visually detected at eddy-current signal levels of 40 to 50 mV, which are much lower than those at rivets A22 and A23. The type of rivets, the joint configuration, and the local residual stress field are some of the factors that may have contributed to this discrepancy. Further studies are needed to gain a better understanding of the phenomenon.

(c) Crack Growth Histories and Growth Rate

The RCCM system was used to take visual crack length measurements. All measurements were taken while holding the panel at 50% full load. Figure 12 shows the crack length vs number of full-load cycles for the four cracks from the left and right sides of rivets A22 and A23, denoted by A22L, A22R, A23L, and A23R. The solid symbols indicate crack growth prior to linking up with the rivet. The open symbols indicate crack growth after linking up with the rivet. Since each crack grew in both directions before it linked up with the rivet hole, the initial growth rate shown as the solid symbols in Figure 12 appears to be much higher than after the crack grew into the rivet hole shown by the open symbols.

After the cracks linked up with the rivet, the subsequent crack growth behavior was similar for the four cracks. To further investigate this phenomena, the crack growth rates of each crack was calculated using the secant method [9]

$$\frac{da}{dN} = \frac{a_{i+1} - a_i}{N_{i+1} - N_i} \tag{3}$$

where:

a = crack length

N = number of load cycles

Figure 13 shows the calculated growth rates vs the average crack length for all four cracks after they have linked up with the rivet holes. The average crack length is defined as:

$$a_{avg} = \frac{a_{i+1} + a_i}{2} \tag{4}$$

Also shown in the figure are data from a flat panel study [8] and a curved panel test [10]. It can be seen that the results obtained in this study, although for longer crack lengths and different joint and panel configurations, follow the trend of both reference data very well. All the data plotted in Figure 13 shows linear type behavior of crack growth rate as a function of the crack length on a log-log scale. This suggests that the fatigue cracks from these three different studies grew at similar rates. A posttest fractographic study will be conducted to provide data in shorter crack length range for further comparison and verification.

Concluding Remarks

A study of multiple-site damage (MSD) initiation, distribution, and linkup in an initially undamaged curved fuselage panel containing a longitudinal lap joint is being conducted. The test is being conducted using the Full-Scale Aircraft Structural Test Evaluation and Research facility located at the Federal Aviation Administration William J. Hughes Technical Center. Quasi-static tests were conducted first to ensure a proper load introduction to the panel. Test results revealed a high local bending deformation along the critical outer rivet row A in the lap joint area, which may be responsible for causing MSD crack initiation in that area. The experimental data were verified by geometrically nonlinear finite element analyses.

The curved panel was subjected to a fatigue loading with a marker band spectrum. During the fatigue test, rivets in the panel were periodically inspected for cracks using the Rotating Eddy-Current Probe system and the Remote Control Crack Monitoring system. High eddy-current signals were

recorded at rivets along the critical outer rivet row A of the lap joint prior to visual detection of skin cracks. All the skin cracks along rivet row A were initially observed at a distance from the edge of the rivet hole, possibly due to the high residual stress field in the vicinity of the rivet head resulting from the riveting process. These cracks propagated back towards the rivets and eventually grew into the rivet holes. Other MSD cracks were observed at rivets holding the shear clips to the skin at the shear clip cutouts located at the frame-stringer intersections.

Crack growth rates were calculated for two sets of MSD cracks, results agreed very well with those from other similar studies. The fatigue test will continue until the first linkup of MSD cracks occurs. The panel will then be subjected to a quasi-static load to failure to determine the residual strength. Posttest fractographic studies will be conducted to reconstruct and map the crack growth histories.

Acknowledgement

The first and the last three authors would like to express their sincere appreciation to the FAA William J. Hughes Technical Center for its support through the FAA-Drexel Fellowship Research Grant (97-G-032) to Drexel University.

REFERENCES

[1] J. McGuire and J. Foucault; 1999; Recommendations for Regulatory Action to Prevent Widespread Fatigue Damage in the Commercial Airplane Fleet; Final Report of the Airworthiness Assurance Working Group.

[2] National Transportation Safety Board, Aircraft Accident Report; Aloha Airlines, Flight 243 Boeing 737-200, N73711, Near Maui, Hawaii April 28, 1988; NTSB/AAR-89/03, 1989.

[3] J. G. Bakuckas, Jr., E. Akpan, P. Zhang, C. A. Bigelow, P. Tan, J. Awerbuch, A. Lau, and T. Tan; 1999; Experimental and Analytical Assessment of Multiple-Site Cracking in Aircraft Fuselage Structure; *Proceedings of 20th Symposium of the International Committee on Aeronautical Fatigue*; Seattle, Washington.

[4] J. G. Bakuckas, Jr.; 2002; Full-Scale Testing and Analysis of Fuselage Structure Containing Multiple Cracks; FAA William J. Hughes Technical Center, Atlantic City International Airport, NJ; DOT/FAA/AR-01/46.

[5] B. Wincheski, J. Simpson, and R. Todhunter; 1997; A New Instrument for the Detection of Fatigue Cracks Under Airframe Rivets; *Review of Progress in Quantitative NDE*; Vol. 16B; pp. 2113-2121.

[6] T. Swift; 1970; Development of the Fail-Safe Design Features of the DC-10; *American Society of Testing and Materials Special Technical Publication 486*;, pp. 164-214.

[7] A. A. Ahmed, J.G. Bakuckas, Jr., C. A. Bigelow, P. Tan, J. Awerbuch, A. Lau, and T. Tan; 2001; Initiation and Distribution of Fatigue Cracks in a Fuselage Lap Joint Curve Panel; *Proceedings of the 5th Aging Aircraft Conference*; Orlando, FL.

[8] S. A. Fawaz; 2000; Equivalent Initial Flaw Size Testing and Analysis; AFRL-VA-WP-TR-2000-3024.

[9] 1992 Annual Book of ASTM Standards; Section 3, Vol. 03.01, pp. 696.

[10] R. S. Piascik, and S. A. Willard; 1997; The Characteristics of Fatigue in the Fuselage Riveted Lap Splice Joint; NASA/TP-97-206257.

Table 1. Applied loads

Test Type	Load Type	Maximum Load			
		Pressure (psi)	Hoop (lb/in)	Frame (lb/in)	Long. (lb/in)
Strain Survey	Quasi-Static	16.0	878.6	177.4	0
Strain Survey	Quasi-Static	0	0	0	528.0
Strain Survey	Quasi-Static	16.0	878.6	177.4	528.0
Fatigue	Cyclic (R=0.1)	16.0	878.6	177.4	528.0

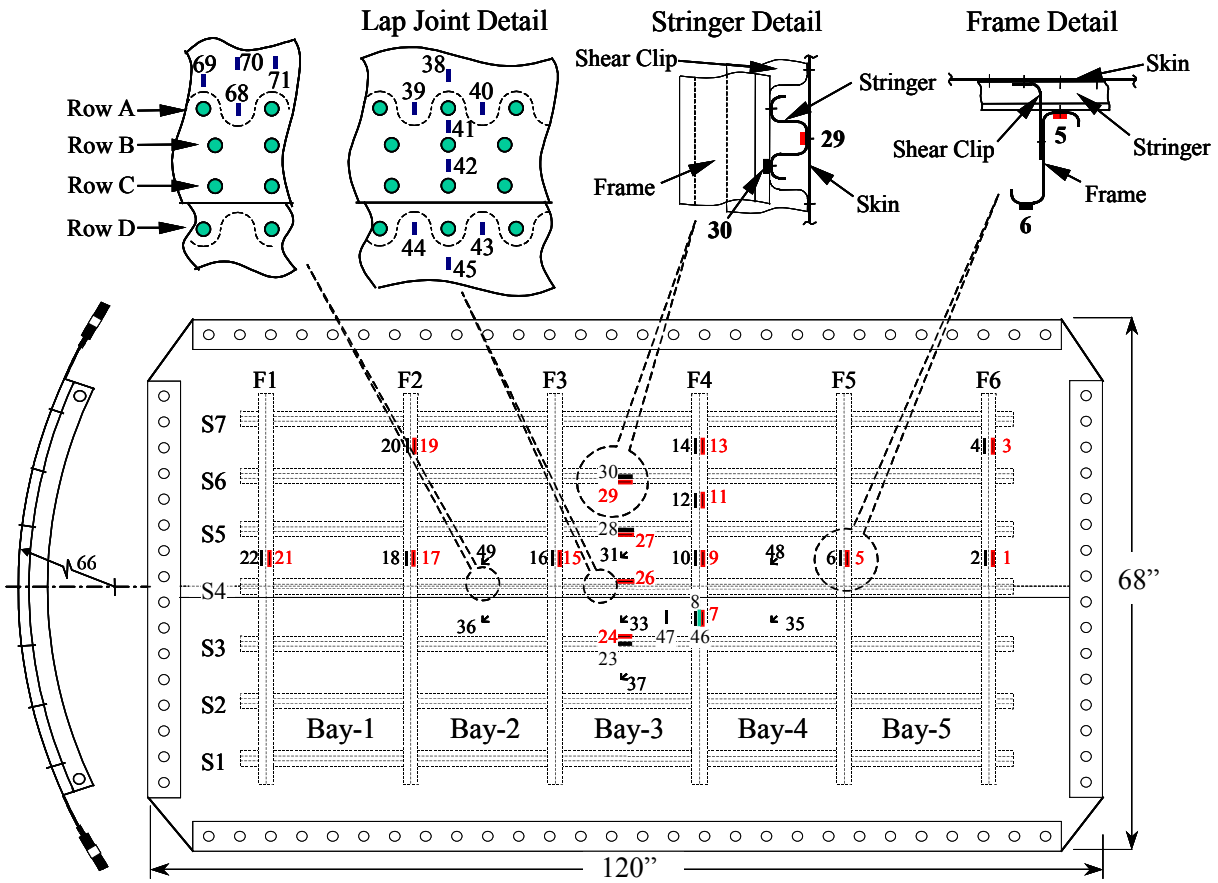

Figure 1. Curved panel dimensions and strain gage locations

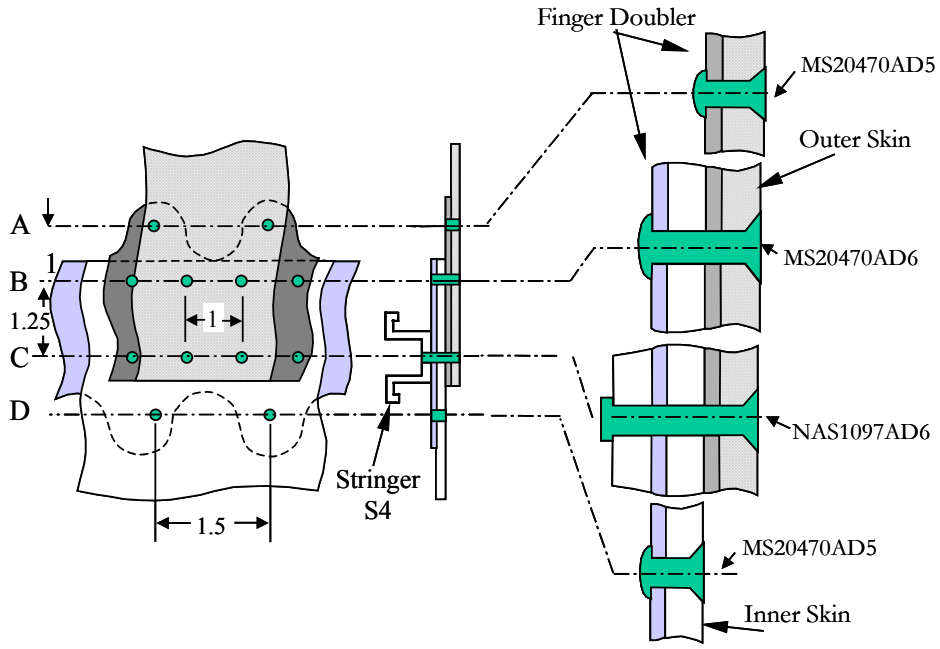

Figure 2. Details of the lap joint and fastener types

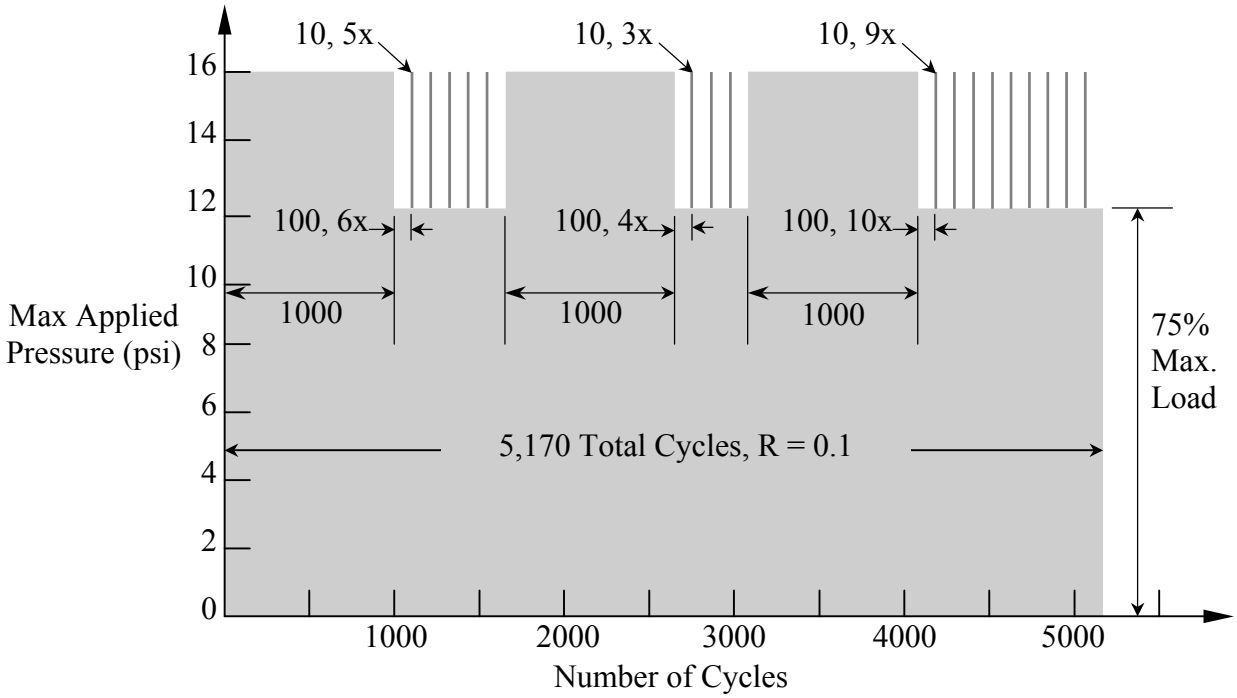

Figure 3. The marker band loading spectrum used in the fatigue test

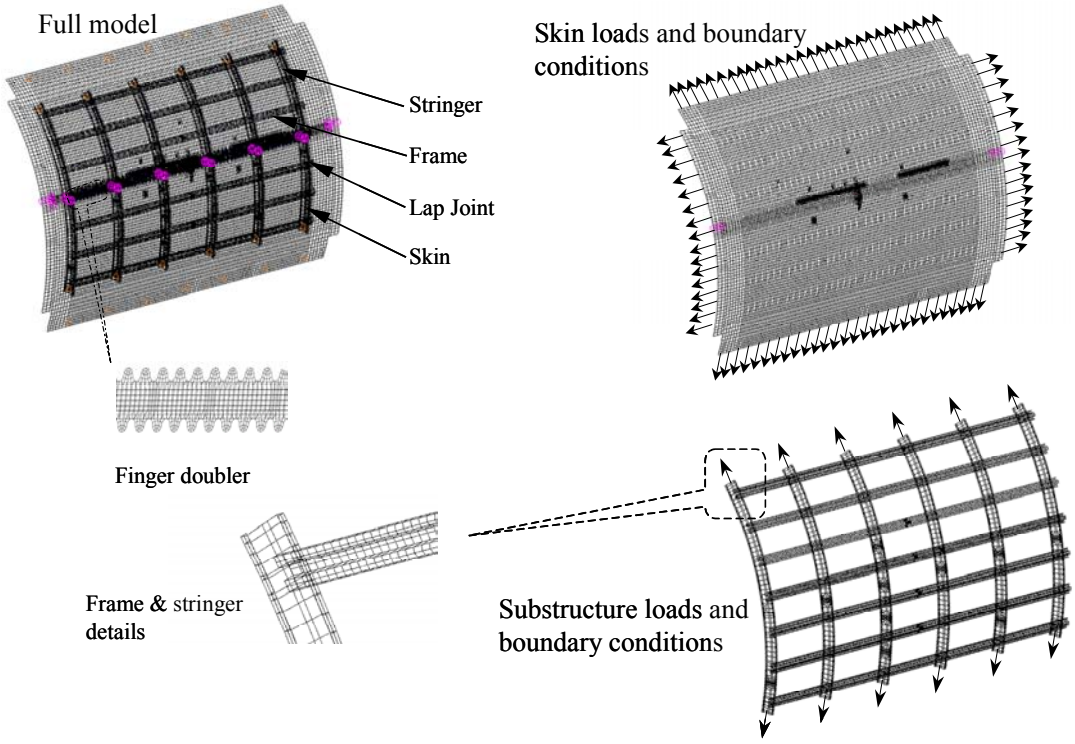

Figure 4. Finite element model of the curved panel with the loadings and boundary conditions

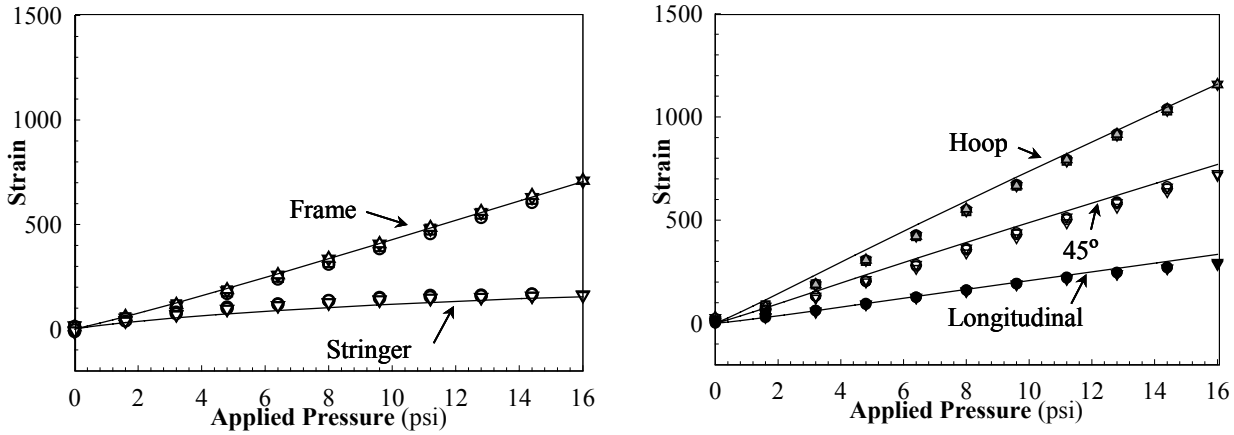

(a) Frame hoop and stringer longitudinal strains

(b) Skin hoop, 45°, and longitudinal strains

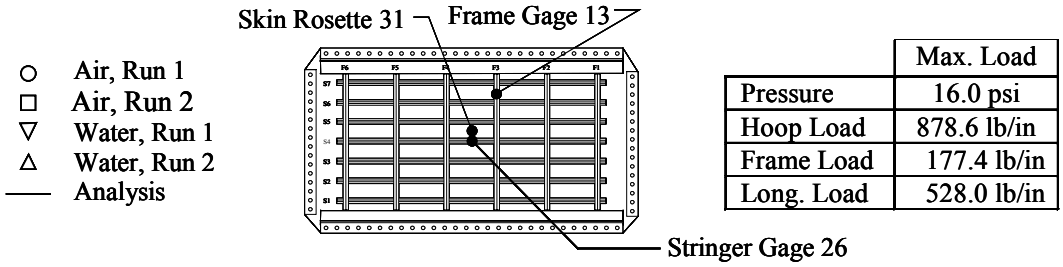

	Max. Load
Pressure	16.0 psi
Hoop Load	878.6 lb/in
Frame Load	177.4 lb/in
Long. Load	528.0 lb/in

Figure 5. Comparison of the experimental data and the FEM predictions for strains at representative strain gage locations

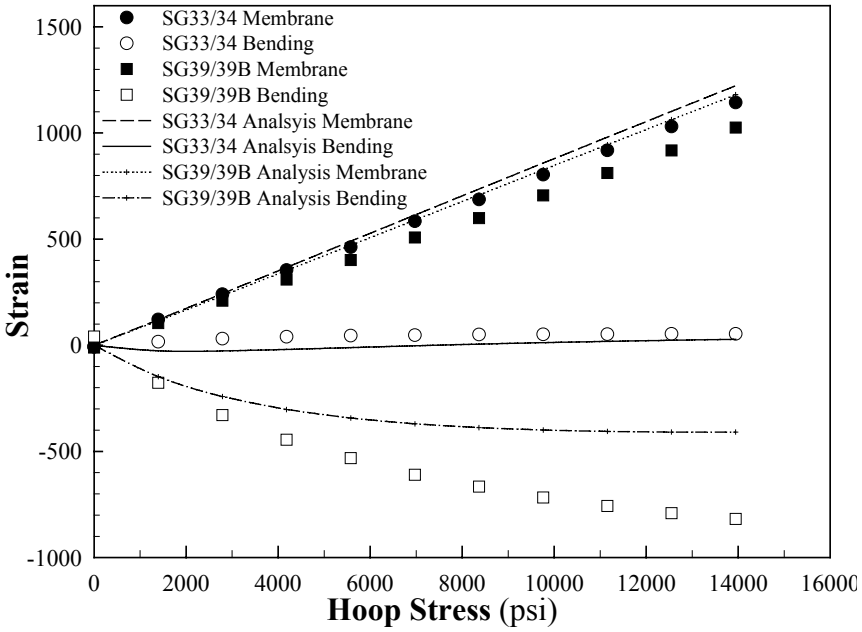

Figure 6. Comparison of membrane and bending strain components measured in the skin midbay (SG33/34) and at rivet row A (SG39/39B). Also shown are FEM analysis predictions

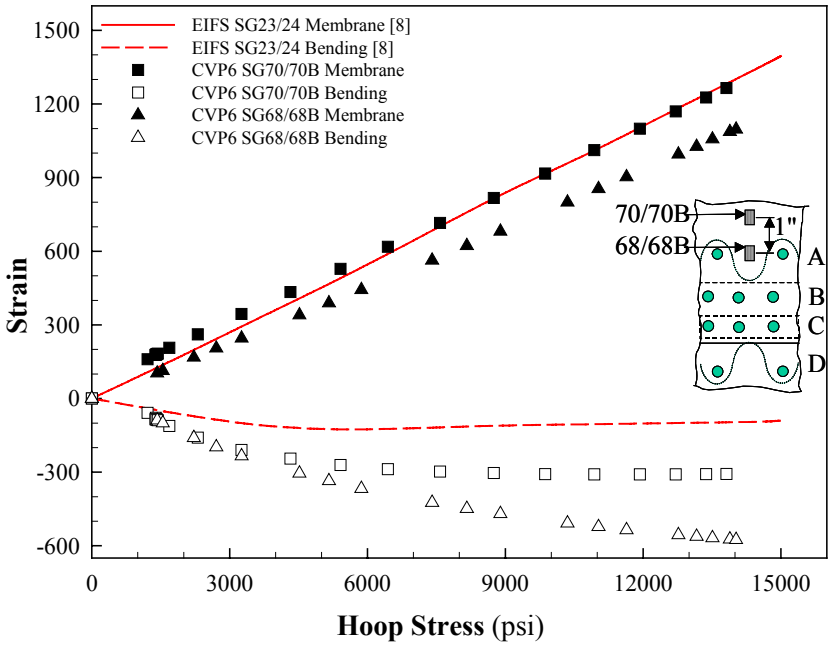

Figure 7. Comparison of the strains measured at the lap joint in the curved panel and in a flat panel

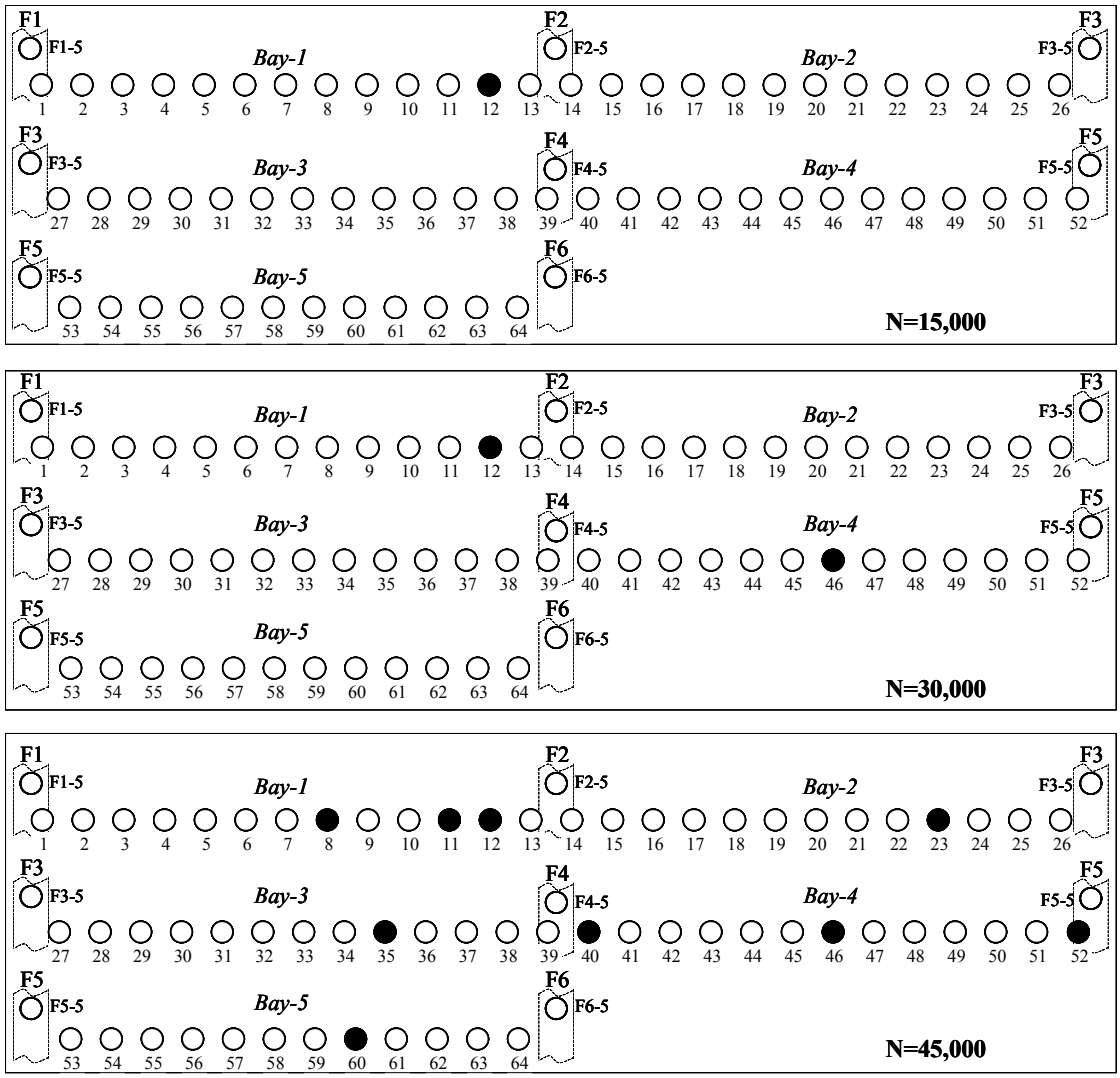

○ ≡ Rivet showing eddy-current signals below the 15 mV threshold
● ≡ Rivet showing eddy-current signal exceeding the 15 mV threshold
◉ ≡ Rivet showing high eddy-current signal and having a head crack
●↖ ≡ Through-the-thickness skin crack emanating from the rivet hole
N ≡ Number of full-load cycles

Figure 8. The damage evolution of rivet row A and the critical shear clip rivets as a function of number of full-load cycles

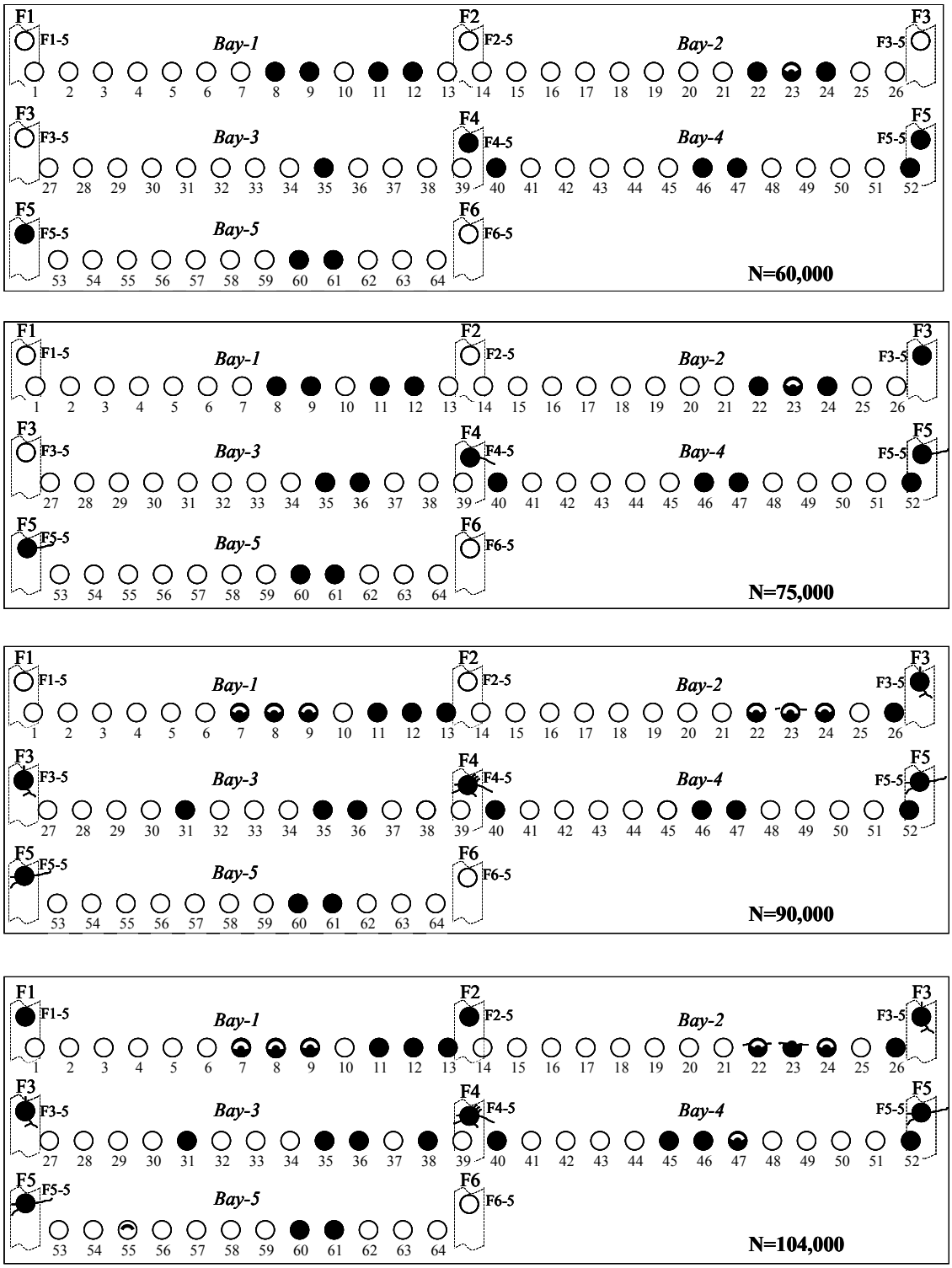

Figure 8. The damage evolution of rivet row A and the critical shear clip rivets as a function of number of full-load cycles (continued)

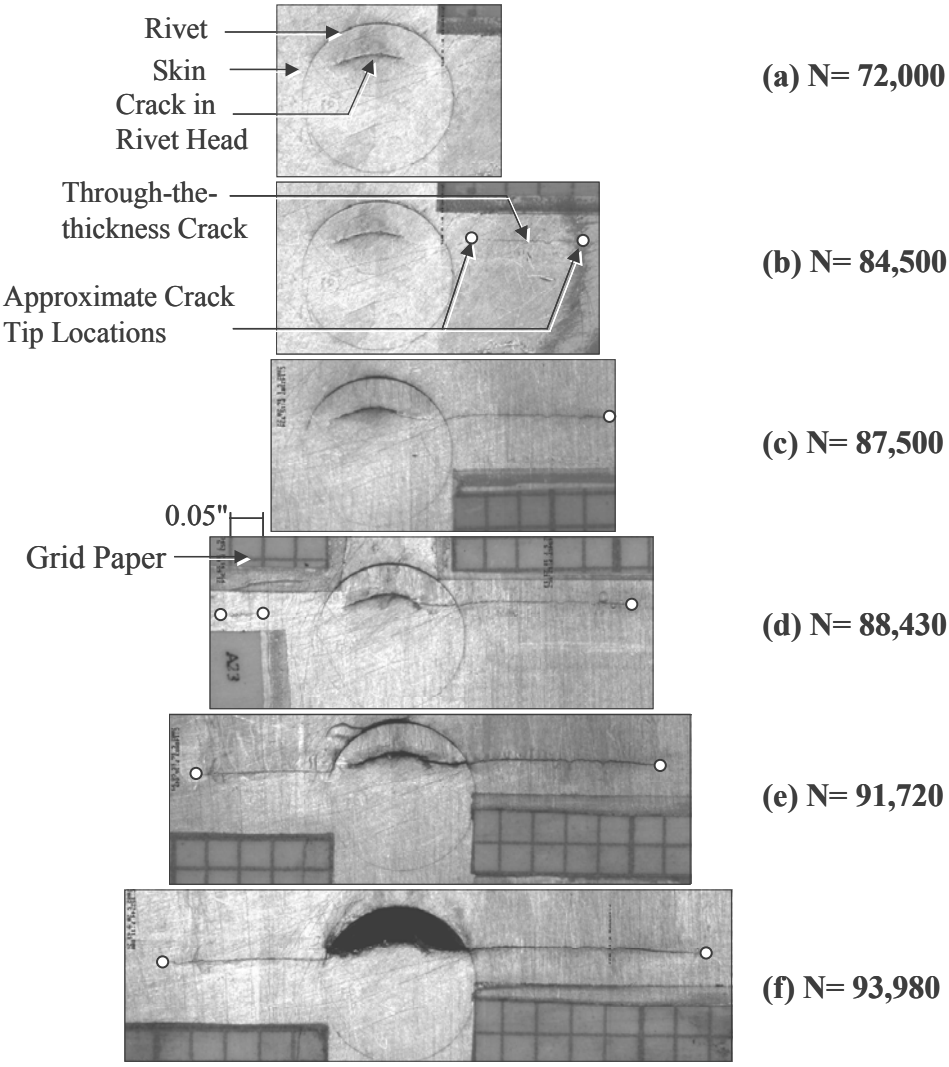

Figure 9. RCCM images showing the damage evolution at rivet A23 as a function of number of full-load cycles (N)

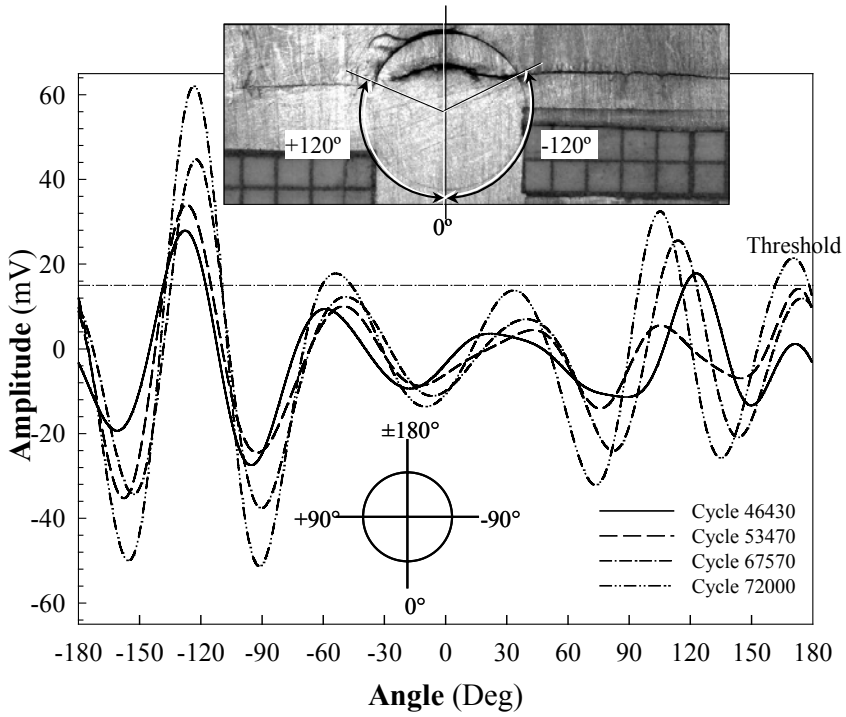

Figure 10. Eddy-current inspection results for rivet A23

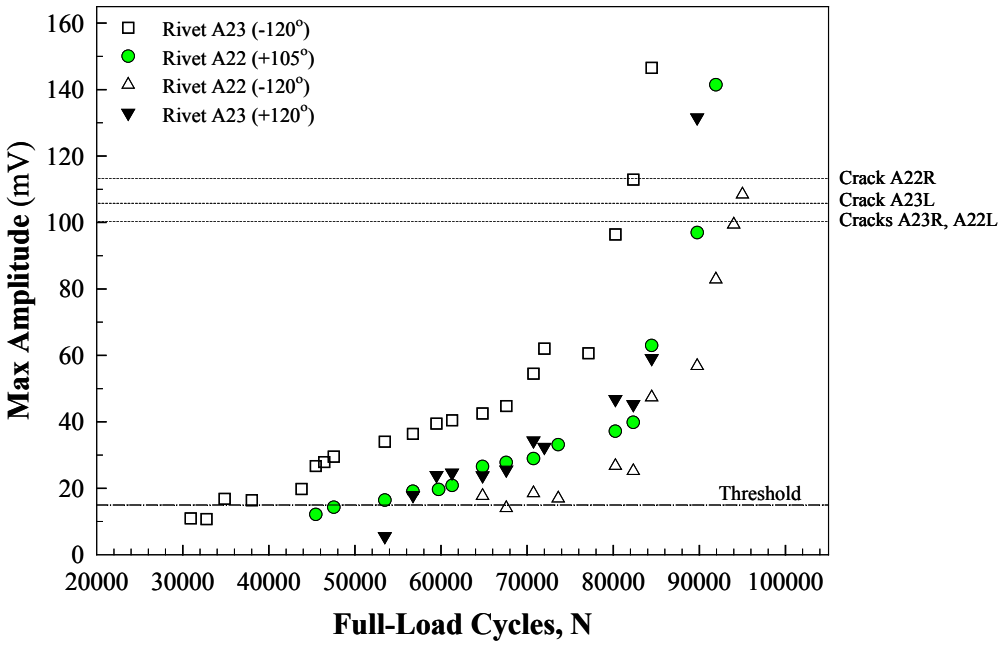

Figure 11. Eddy-current maximum signal versus number of full-load cycles for rivets A22 and A23

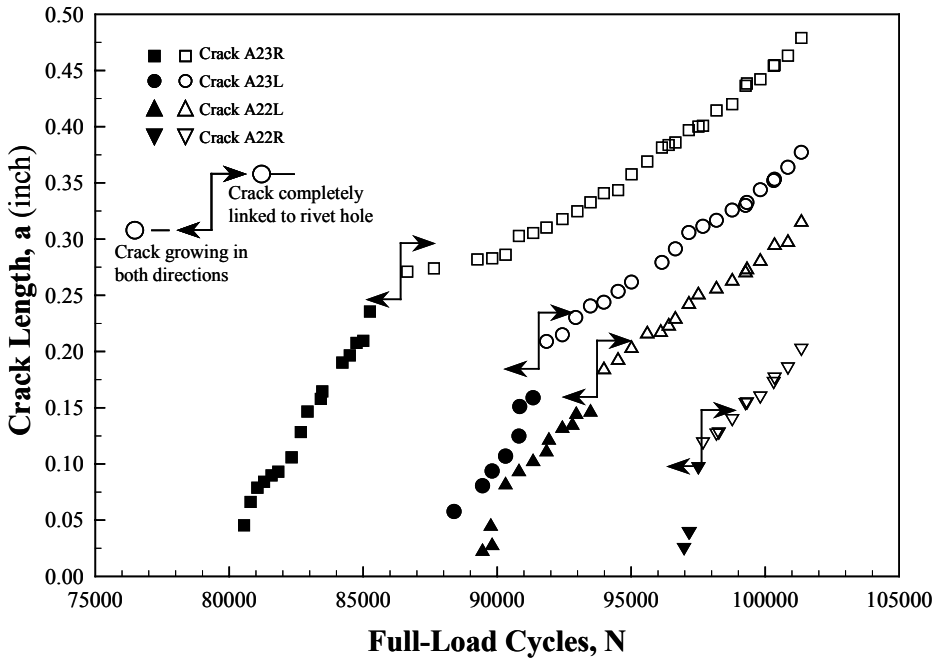

Figure 12. Crack length versus number of full-load cycles for cracks initiated at rivets A22 and A23

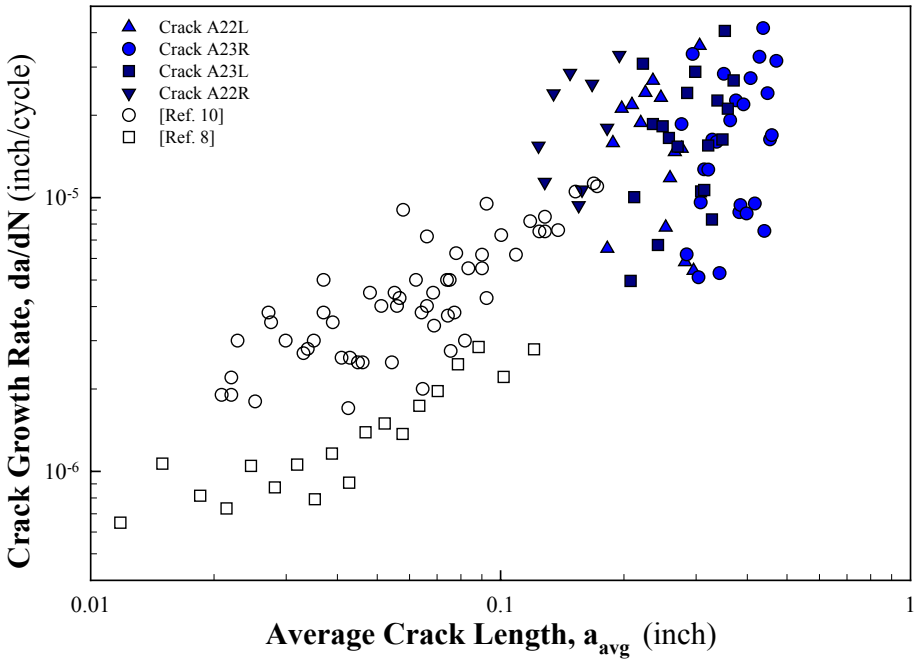

Figure13. Crack growth rates for the lap joint cracks